The Plant Cell, Vol. 29: 1105–1118, May 2017, www.plantcell.org © 2017 ASPB.

KNOTTED1 Cofactors, BLH12 and BLH14, Regulate Internode Patterning and Vein Anastomosis in Maize[OPEN]

Katsutoshi Tsuda,[a,b] Maria-Jazmin Abraham-Juarez,[c,1] Akiteru Maeno,[d,1] Zhaobin Dong,[c] Dale Aromdee,[c] Robert Meeley,[e] Toshihiko Shiroishi,[b,d] Ken-ichi Nonomura,[a,b] and Sarah Hake[c,1,2]

[a] Experimental Farm, National Institute of Genetics, Mishima, Shizuoka 411-8540, Japan
[b] Department of Genetics, School of Life Science, Graduate University for Advanced Studies, Mishima, Shizuoka 411-8540, Japan
[c] Plant Gene Expression Center, U.S. Department of Agriculture-Agricultural Research Service, Plant and Microbial Biology Department, University of California at Berkeley, Albany, California 94710
[d] Mammalian Genetics Laboratory, National Institute of Genetics, Mishima, Shizuoka, 411-8540, Japan
[e] Pioneer Hi-Bred International, Johnston, Iowa 50131

ORCID IDs: 0000-0001-6325-5201 (K.T.); 0000-0002-5468-8176 (M.-J.A.-J.); 0000-0002-4496-1888 (R.M.); 0000-0002-2057-543X (K.N.); 0000-0001-6953-1529 (S.H.)

Monocot stems lack the vascular cambium and instead have characteristic structures in which intercalary meristems generate internodes and veins remain separate and scattered. However, developmental processes of these unique structures have been poorly described. BELL1-like homeobox (BLH) transcription factors (TFs) are known to heterodimerize with KNOTTED1-like homeobox TFs to play crucial roles in shoot meristem maintenance, but their functions are elusive in monocots. We found that maize (*Zea mays*) BLH12 and BLH14 have redundant but important roles in stem development. BLH12/14 interact with KNOTTED1 (KN1) in vivo and accumulate in overlapping domains in shoot meristems, young stems, and provascular bundles. Similar to *kn1* loss-of-function mutants, *blh12 blh14* (*blh12/14*) double mutants fail to maintain axillary meristems. Unique to *blh12/14* is an abnormal tassel branching and precocious internode differentiation that results in dwarfism and reduced veins in stems. Micro-computed tomography observation of vascular networks revealed that *blh12/14* double mutants had reduced vein number due to fewer intermediate veins in leaves and precocious anastomosis in young stems. Based on these results, we propose two functions of BLH12/14 during stem development: (1) maintaining intercalary meristems that accumulate KN1 and prevent precocious internode differentiation and (2) preventing precocious anastomosis of provascular bundles in young stems to ensure the production of sufficient independent veins.

INTRODUCTION

Plant architecture results from the repeated production of lateral organs from the shoot apex in coordination with growth of the stem, a cylindrical supporting structure beneath the shoot apex. Growth of the stem separates the lateral organs, allowing for more efficient light reception and gas exchange. Stems also provide mechanical support, which is particularly enhanced by the rigid, lignified cells in the vascular system that connects water-absorbing roots with photosynthetic aerial organs. In crop species, regulation of stem elongation is particularly important because of its impact on potential yield loss due to lodging. Thus, stem growth has been a major target of crop improvement as exemplified by semidwarf mutations in the phytohormone gibberellin pathway that were utilized in the green revolution (Hedden, 2003). Despite the importance, however, developmental processes of stems and its underlying mechanisms are poorly characterized.

Stem growth occurs in an interrupted pattern between initiating leaves. The region of growth is referred to as the internode, whereas the node is the site of leaf attachment. From clonal analysis, it appears that the node and the subtending internode arise from the same pool of cells (Johri and Coe, 1983). Growth in the internode is basipetal in most species (Kaplan, 2000). This growth pattern places the meristematic zone of one internode, called the intercalary meristem, just above the node of the subtending leaf.

Monocotyledonous plants are named for the difference in their embryonic leaves but are also distinguished by their stem venation pattern. Dicotyledonous plants have the vascular cambium and produce a ring of vasculature, known as a eustele, with the xylem on the inside and phloem on the outside. Monocots lack the vascular cambium and instead have what is referred to as a scattered venation pattern (or atactostele) (Sanchez et al., 2012). Monocots and dicots also differ in how veins enter from leaves into stems. In a typical dicot leaf, the reticulate venation coalesces into a major vein that enters into the stem and anastomoses with the ring of vasculature. In many monocots, but specifically in grasses, the parallel veins of the leaf each enter into the stem without coalescence and become individual veins that are scattered in the stem. This venation pattern in monocots provides a unique opportunity to study the mechanism that regulates vein anastomosis.

Three amino acid loop extension (TALE) homeodomain transcription factors (TFs) are conserved throughout eukaryotes and have essential roles in diverse developmental contexts (Bürglin and Affolter, 2016; Tsuda and Hake, 2015). In plants, TALE TFs are classified into two subfamilies, KNOTTED1-like homeobox

[1] These authors contributed equally to this work.
[2] Address correspondence to hake@berkeley.edu.
The author responsible for distribution of materials integral to the findings presented in this article in accordance with the policy described in the Instructions for Authors (www.plantcell.org) is: Sarah Hake (hake@berkeley.edu).
[OPEN] Articles can be viewed without a subscription.
www.plantcell.org/cgi/doi/10.1105/tpc.16.00967

(KNOX) and BELL1-like homeobox (BLH). KNOX and BLH proteins interact to produce functional heterodimers most famously demonstrated by their role in zygote development in *Chlamydomonas reinhardtii* (Lee et al., 2008). In flowering plants such as *Arabidopsis thaliana*, *BLH* genes are involved in various developmental processes including shoot meristem maintenance, lateral organ patterning, and carpel development (Reiser et al., 1995; Kumar et al., 2007; Rutjens et al., 2009; Byrne et al., 2003; Bhatt et al., 2004; Roeder et al., 2003; Smith and Hake, 2003). However, their function in monocot species has not been described.

We investigated the maize (*Zea mays*) homologs of Arabidopsis PENNYWISE, BLH12 and BLH14. Both proteins interact with KN1 and accumulate in shoot meristems, young stems, intercalary meristems, and provascular bundles. The double mutants lacked tillers and ears and had highly branched tassels. Strikingly, the intercalary meristems failed to be maintained and the stem provascular bundles precociously anastomosed, indicating important roles for TALE TFs in vasculature and internode patterning in the stem.

RESULTS

Maize PNY homologs, BLH12 and BLH14, Interact with KN1

Eighteen BLH proteins were identified from database searches in the maize genome. Phylogenetic analysis using an additional 13 BLHs from Arabidopsis identified three maize proteins, BLH12, BLH13, and BLH14, as close homologs of Arabidopsis PENNYWISE (PNY) (Figure 1A). Similar to *PNY*, all three maize genes are expressed at high levels in shoot meristems including the shoot apical meristem (SAM), young tassels, and ears and at lower levels in leaves (Supplemental Figure 1). Given that *blh13* expression level is relatively low compared with the other two genes, our analysis focuses on *blh12* and *blh14*.

Mutator (*Mu*) insertions were obtained for *blh12* and *blh14*. The insertions are in the 5′ untranslated region, exon 2, and exon 4 in *blh12-1*, *blh12-3*, and *blh12-2*, respectively (Figure 1B). An immunoblot using an anti-BLH12 antibody revealed that the accumulation of BLH12 protein in the vegetative shoot apex was lost in *blh12-1* and *blh12-3* and greatly reduced in *blh12-2* (Figure 1C). Similarly, an immunoblot using an anti-BLH14 antibody did not detect BLH14 protein in shoot apices of *blh14-1*, which contains a *Mu* insertion in exon 1 of *blh14*. Thus, these *Mu* insertion lines are loss-of-function mutants of *BLH12* and *BLH14*.

PNY interacts with the Arabidopsis KNOX protein SHOOTMERISTEMLESS (Byrne et al., 2003; Smith and Hake, 2003). To test if BLH12 and BLH14 have the potential to interact with KN1, a bimolecular fluorescence complementation (BiFC) assay was performed in *Nicotiana benthamiana* leaves. The C-terminal half of YFP was fused to the N terminus of BLH12 and BLH14. When these proteins were transiently expressed with KN1 fused to the N-terminal half of YFP, the fluorescence was recovered in nuclei, indicating both BLH12 and BLH14 interact with KN1 (Figure 1D). We further tested if these BLHs interact with KN1 in vivo by coimmunoprecipitation using shoot apices. After immunoprecipitation by anti-BLH12 antibody, KN1 protein was detected in the wild type, but not in the *blh12-3* single mutant (Figure 1E). Similarly, KN1 was also detected in the anti-BLH14 immunoprecipitate of the wild type, but not the *blh14-1* mutant (Figure 1F). These results demonstrate that BLH12 and BLH14 are bona fide cofactors of KN1.

BLH12 and BLH14 Localization Overlaps with That of KN1

BLH12 and BLH14 accumulation patterns were observed in developing tissues by immunostaining. As negative controls, anti-BLH12 and anti-BLH14 antibodies were reacted with *blh12-3* and *blh14-1* mutants, respectively (Figures 2B and 2E). No staining was detected, confirming that these antibodies are specific.

In vegetative shoot apices, BLH12 was detected in axillary meristems and provascular bundles in the unexpanded stem. Accumulation was weak in the plastochron 0 (P0) leaf primordium but stronger just above it (Figure 2A). BLH12 was not detected in older leaf primordia. BLH12 expression in the apical part of the SAM was usually absent, although it was occasionally detected (4 out of 15 observations; Supplemental Figures 2A and 2B).

BLH14 accumulated to high levels in axillary meristems, provascular bundles, and the SAM. In contrast to BLH12, BLH14 was consistently expressed in the SAM and was downregulated in the P0 (Figure 2D). Low accumulation was occasionally detected in the abaxial epidermis in young leaf primordia. As previously reported (Johnston et al., 2014), BLH14 was detected in the preligule (Supplemental Figures 2C and 2D). Both BLH12 and BLH14 were found in cells destined to become axillary meristems (Figures 2C and 2F).

To confirm that the BLHs are expressed in domains overlapping with KN1, we performed immunostaining on serial sections of young tassels with antibodies against BLH12, KN1, and BLH14. As previously reported, KN1 accumulates in provascular bundles and the inflorescence branch and spikelet meristems in tassel primordia (Figures 2H and 2K) (Smith et al., 1992; Jackson et al., 1994). BLH12 accumulation was detected in the inflorescence meristem, the spikelet meristem, and provascular bundles of the rachis (Figures 2G and 2J). Increased BLH12 expression was detected at the boundary between spikelet meristems and differentiating lateral organs, but entire spikelet meristems were also occasionally stained. BLH14 showed a similar accumulation pattern as BLH12, but as in the vegetative meristem, its expression was stronger and more consistent in spikelet meristems (Figures 2I and 2L). Accumulation of BLH14 and KN1 disappeared in the abaxial side of the spikelet meristem, where the bract-like glume initiates (Figures 2K and 2L). BLH12 and BLH14 also accumulate in spikelet meristems of developing ears (Supplemental Figures 2E and 2F). Collectively, BLH12 and BLH14 accumulate in overlapping domains with KN1 in both vegetative and reproductive shoot meristems, suggesting that these BLHs could play important roles in meristem maintenance as KN1 cofactors.

blh12 blh14 Double Mutants Have Short Internodes and Lack Lateral Branches

To study the function of these BLHs in shoot development, mutant phenotypes were analyzed after three introgressions into the standard inbred B73. Because both *blh12-2* and *blh14-1* single

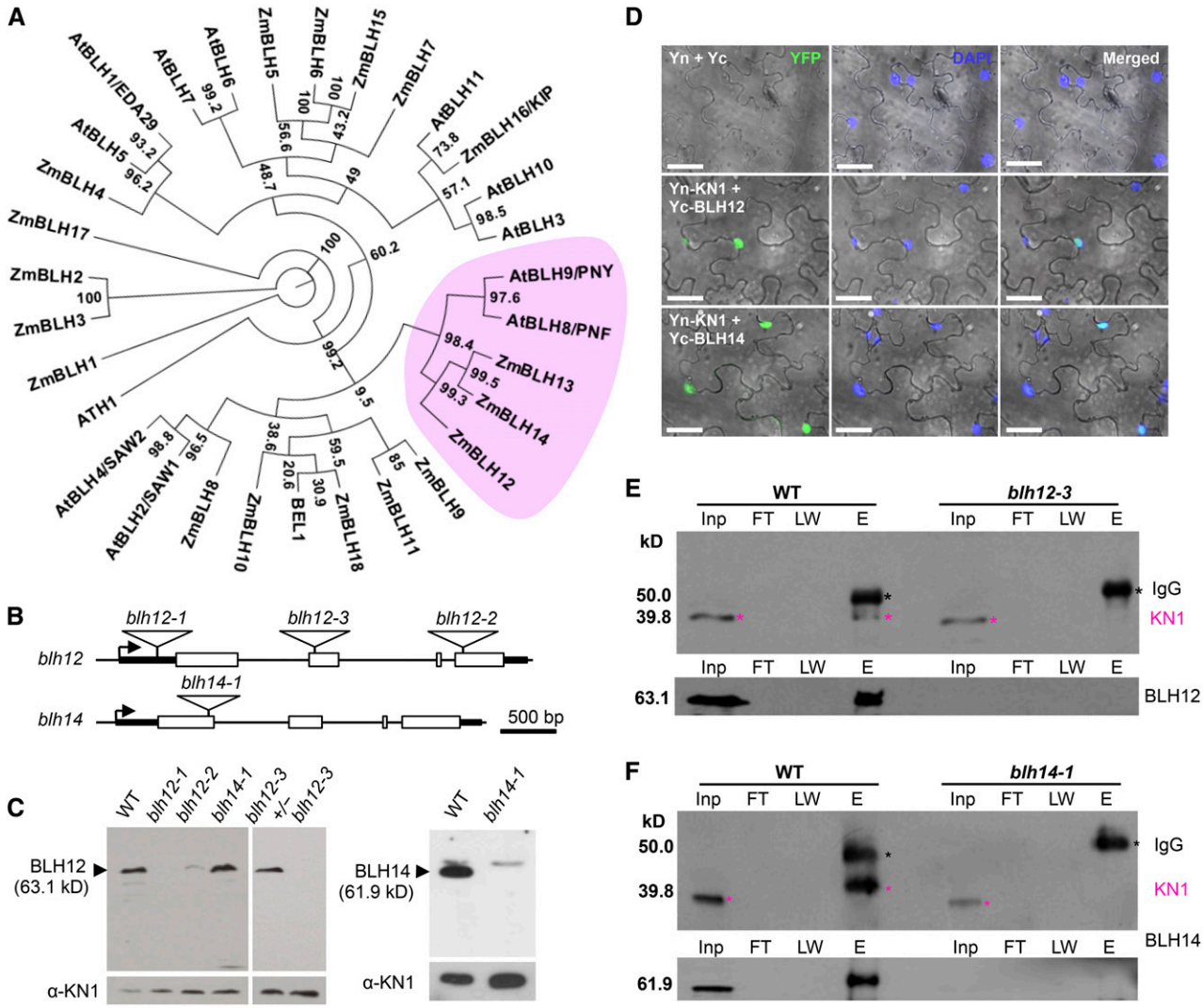

Figure 1. Maize PNY Homologs BLH12 and BLH14 Interact with KN1.

(A) A phylogenic tree of maize and Arabidopsis BLH proteins. The PNY clade is pink. Bootstrap values are indicated at each branch point. Gene IDs and accession numbers are listed in Supplemental Table 3. The alignments used to generate the phylogeny are provided in Supplemental File 1.
(B) *Mutator* insertions in *blh12* and *blh14*. Boxes, triangles, arrows, and thick lines indicate exons, *Mutator* transposons, transcription start sites, and 5′ or 3′ untranslated regions, respectively. Thin lines represent other regions including up- and downstream regions and introns.
(C) Immunoblots for BLH12 (left) and BLH14 (right) using protein extracts from shoot apices of 3-week-old seedlings. KN1 was used as a loading control (bottom). WT, wild type.
(D) BiFC assay showing interactions between KN1 and BLH12 or BLH14 in planta. *Agrobacterium tumefaciens* lines containing constructs shown on the left were infiltrated into *N. benthamiana* leaves. Three biological replicates (~100 nuclei for each replicate) were observed and fluorescence was detected in ~25% of nuclei. Confocal images were overlaid on the bright field. Yn and Yc represent YFP N-terminal half and C-terminal half, respectively. Bars = 40 μm.
(E) and **(F)** Protein coimmunoprecipitation of KN1 with BLH12 **(E)** or BLH14 **(F)**. Protein extracts from shoot apices were immunoprecipitated using anti-BLH12 or anti-BLH14 antibodies followed by immunoblots using anti-KN1 (top), anti-BLH12 (bottom in **[E]**), or anti-BLH14 (bottom in **[F]**) antibodies. Black and magenta asterisks indicate IgG heavy chains and KN1, respectively. KN1 immunoprecipitated with BLH14 runs at a higher molecular weight, possibly due to posttranslational modifications. Inp, total inputs. FT, flow-through fractions; LW, washing fractions; E, eluted fractions.

mutants were normal except for slightly narrower leaf blades observed in *blh12-2* (Supplemental Figure 3A), double mutants were observed in segregating progeny of self-pollinated *blh12-2*/+ *blh14-1*/+ double heterozygous plants. In vegetative growth, *blh12-2 blh14-1* double mutants (referred to as *blh12/14* for simplicity) had narrower leaves than *blh12-2* single mutants, indicating BLH14 has a functional redundancy with BLH12 in leaf development. At maturity, *blh12/14* double mutants were clearly shorter than other siblings ($n = 11$; Figures 3A to 3C; Supplemental Figure 3B). Leaf number was almost the same (Supplemental

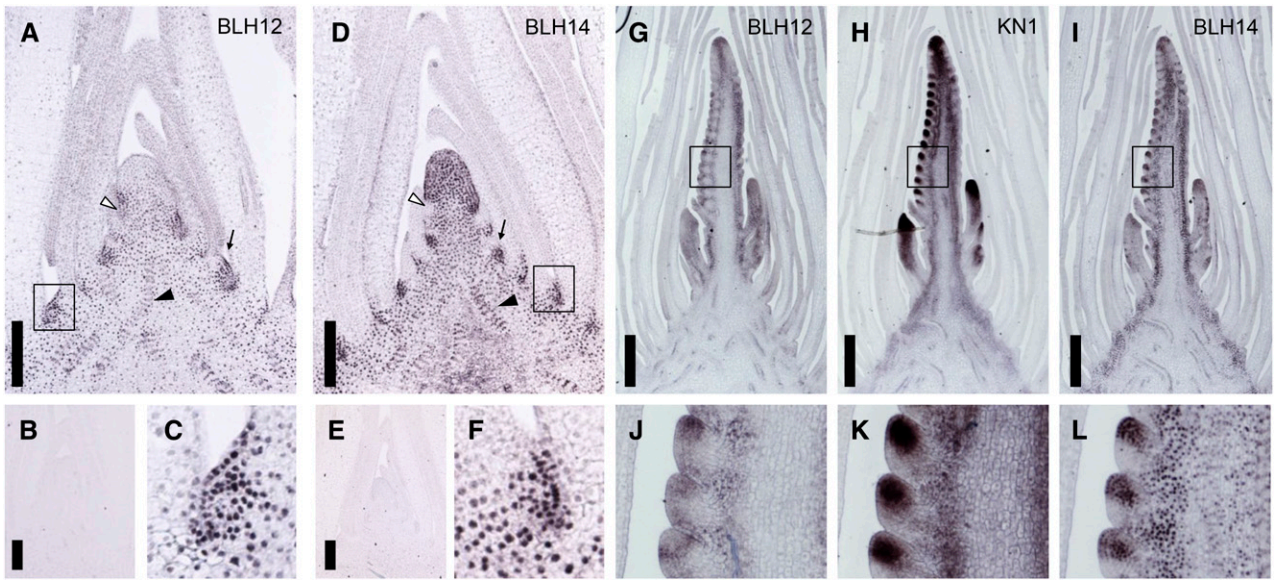

Figure 2. Accumulation Patterns of BLH12 and BLH14.

(A) to **(C)** Immunostainings of BLH12 in the shoot apex. Tissue sections are prepared from the wild type in **(A)** and **(C)** or from *blh12-3* homozygote in **(B)**.
(D) to **(F)** Immunostainings of BLH14 in the shoot apex. Tissue sections were prepared from the wild type in **(D)** and **(F)** or from *blh14-1* homozygote in **(E)**.
Arrows, arrowheads, and open arrowheads indicate axillary meristems, provascular bundles, and P0 leaf primordia, respectively, in **(A)** and **(D)**.
(G) to **(I)** Immunostainings of BLH12 **(G)**, KN1 **(H)**, and BLH14 **(I)** in serial sections of a wild-type young tassel.
(J) to **(L)** Immunostainings of BLH12 **(J)**, KN1 **(K)**, and BLH14 **(L)** in spikelet meristems.
Boxes in **(A)**, **(D)**, and **(G)** to **(I)** represent magnified areas in **(C)**, **(F)**, and **(J)** to **(L)**, respectively. Bars = 200 μm in **(A)**, **(B)**, **(D)**, and **(E)** and 500 μm in **(G)** to **(I)**.

Figure 3C), but internodes were severely shortened compared with normal siblings, especially in the top four to five internodes (Figures 3B to 3D). Double mutants also lacked any axillary branches such as ears or tillers and had severely reduced tassels, leading to complete sterility. In combinations between *blh12-1* or *blh12-3* and *blh14-1*, the same defects were observed only in double mutants, confirming that these abnormalities were caused by loss of both *BLH12* and *BLH14*.

Precocious Elongation and Limited Growth of Internodes in *blh12/14* Double Mutants

During the vegetative stage (4 weeks old), double mutant plants showed no gross abnormalities except for narrower leaves (Supplemental Figures 3A and 4). However, tissue sections revealed that the internodes of double mutants were more elongated compared with the wild type (Figure 4). In wild-type siblings, vertical files of cells first become visible in internodes between P9 and P10 nodes (Figures 4A and 4B, bracket with three asterisks). These vertical files become internode parenchyma cells, whose extensive expansion will be the primary cause of stem elongation (Sharman, 1942). In contrast, these vertical cell files were detected in the internodes between P7 and P8 nodes in the double mutants, suggesting precocious internodal cell differentiation during stem development (Figures 4C and 4D). It is worth noting that radial growth was also impaired in *blh12/14* mutant stems (Figures 4A and 4C).

To examine cell differentiation states during stem development, we analyzed KN1 accumulation. In the wild type, KN1 accumulated in stripes in the young stem (Figure 4E). Higher magnification revealed that KN1 was downregulated in the vertical files of future internodal parenchyma, whereas its accumulation persisted in the nodal region above and below (Figure 4F). The KN1-positive cells with active cell division in the horizontal plane (Figure 4F, bracket with two asterisks) are the presumed intercalary meristem. These results suggest that intercalary meristems and adjacent nodal regions remain indeterminate at a time when the vertical files of internodal cells differentiate. In *blh12/14* mutants, KN1 accumulation was limited to a few nodes just below the SAM and absent in older nodes (Figure 4G). Importantly, the intercalary meristems normally found in the wild type are lost or ambiguous in double mutants (Figures 4A and 4C; see Supplemental Figure 5 for higher magnifications). These results suggest that the intercalary meristem was lost due to precocious internode cell differentiation in double mutants.

Immunostaining of the young stem showed that BLH14 also accumulated in the nodal region but was absent in the internodal vertical cell files (Figures 4H and 4I). BLH12 accumulation was also higher in nodal regions compared with internodes (Supplemental Figure 6). The similarity of accumulation pattern with KN1 suggests that BLH12 and BLH14 maintain an indeterminate state of young nodal cells in concert with KN1.

At 6 weeks old or later, the premature elongation of internodes became visible. Several internodes subtending the tassel were more elongated in double mutants compared with the wild type. However, their precocious elongation plateaued at around the eleventh internode from the tassel, and in the twelfth, the wild-type internode became equivalent to or longer than that of the *blh12/14*

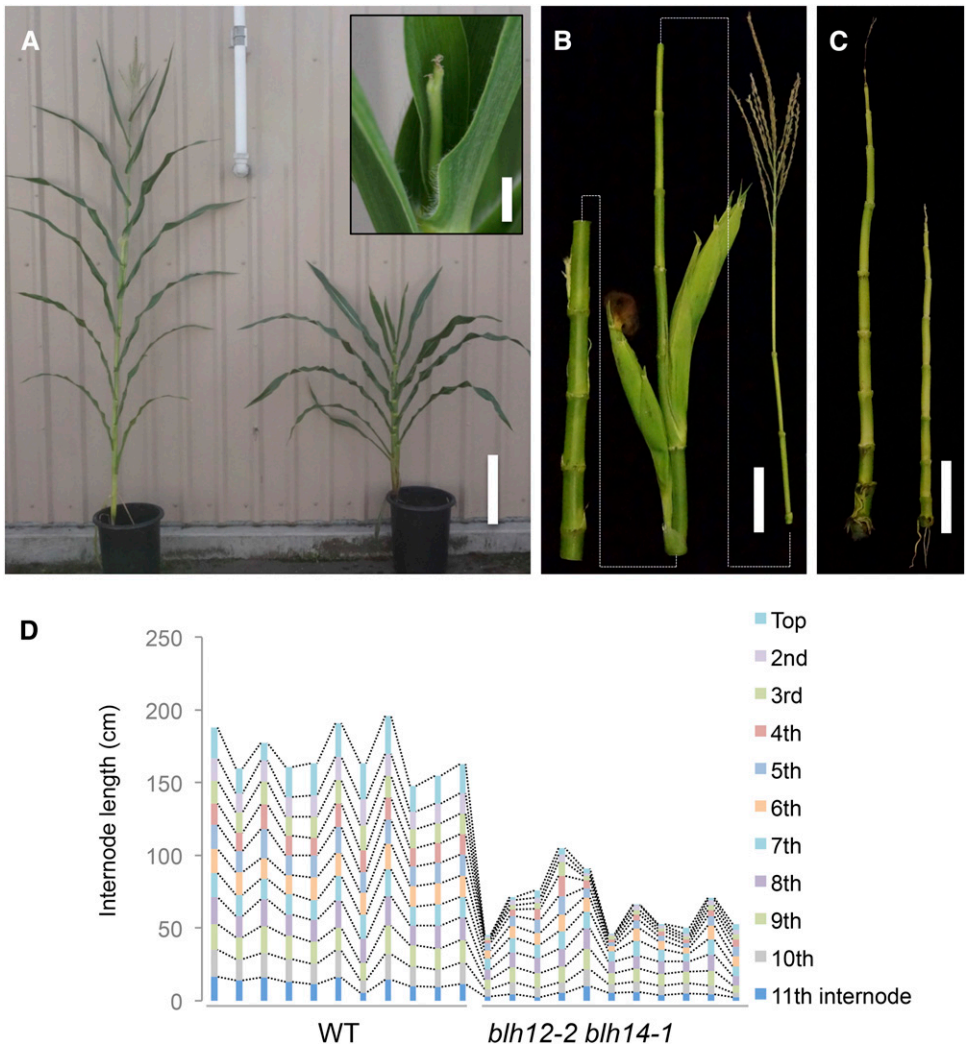

Figure 3. *blh12-2 blh14-1* Double Mutants Show a Dwarf Phenotype.

(A) Mature wild-type (left) and *blh12-2 blh14-1* double mutant plants. *blh12-2 blh14-1* tassel is shown in the inset.
(B) and **(C)** Internodes of the wild type **(B)** and *blh12-2 blh14-1* **(C)**. Leaves are removed from mature plants. Dashed lines in **(B)** represent cut internodes originally connected.
(D) Measurement of internode length. Eleven plants for each genotype were measured. WT, wild type. Bars = 30 cm in **(A)**, 1 cm in the inset, and 10 cm in **(B)** and **(C)**.

mutant (Figures 4J and 4K). Thus, the precociously differentiated internodes of the double mutant lost growth activity prematurely, suggesting that maintenance of the intercalary meristems by BLH12 and BLH14 is essential to achieve full growth potential.

Failure of Axillary Meristem Maintenance

The lack of ears in *blh12/14* mutants suggests a defect in axillary bud initiation or growth. In a family segregating all possible genotypes, no *blh12/14* double mutants had tillers, whereas 30 to 60% of plants of other genotypes produced tillers (Supplemental Table 1). This result showed that BLH12 and BLH14 have redundant functions essential for axillary bud development throughout vegetative and reproductive development.

To understand the basis for the axillary meristem defect, we observed shoot apices at younger stages. At 6 weeks, the absence of an axillary bud was already clear in double mutants (Figure 5A). Occasionally, a single elongated prophyll was observed, but with no axillary meristem. Tissue sections of 4-week-old *blh12/14* plants revealed that, in leaf axils, deeply stained nucleocytoplasmic cells were initially formed, but were lost in P7 or older leaf axils, suggesting that axillary meristems were initiated but could not be maintained (Figures 4A and 4C; Supplemental Figures 7A to 7D). Indeed, KN1 was detected in the axils of the youngest leaf primordia, but its accumulation gradually weakened and was lost in P6 or later stages (Supplemental Figures 7E and 7F). These observations show that BLH12 and BLH14 play essential roles in maintaining axillary meristems.

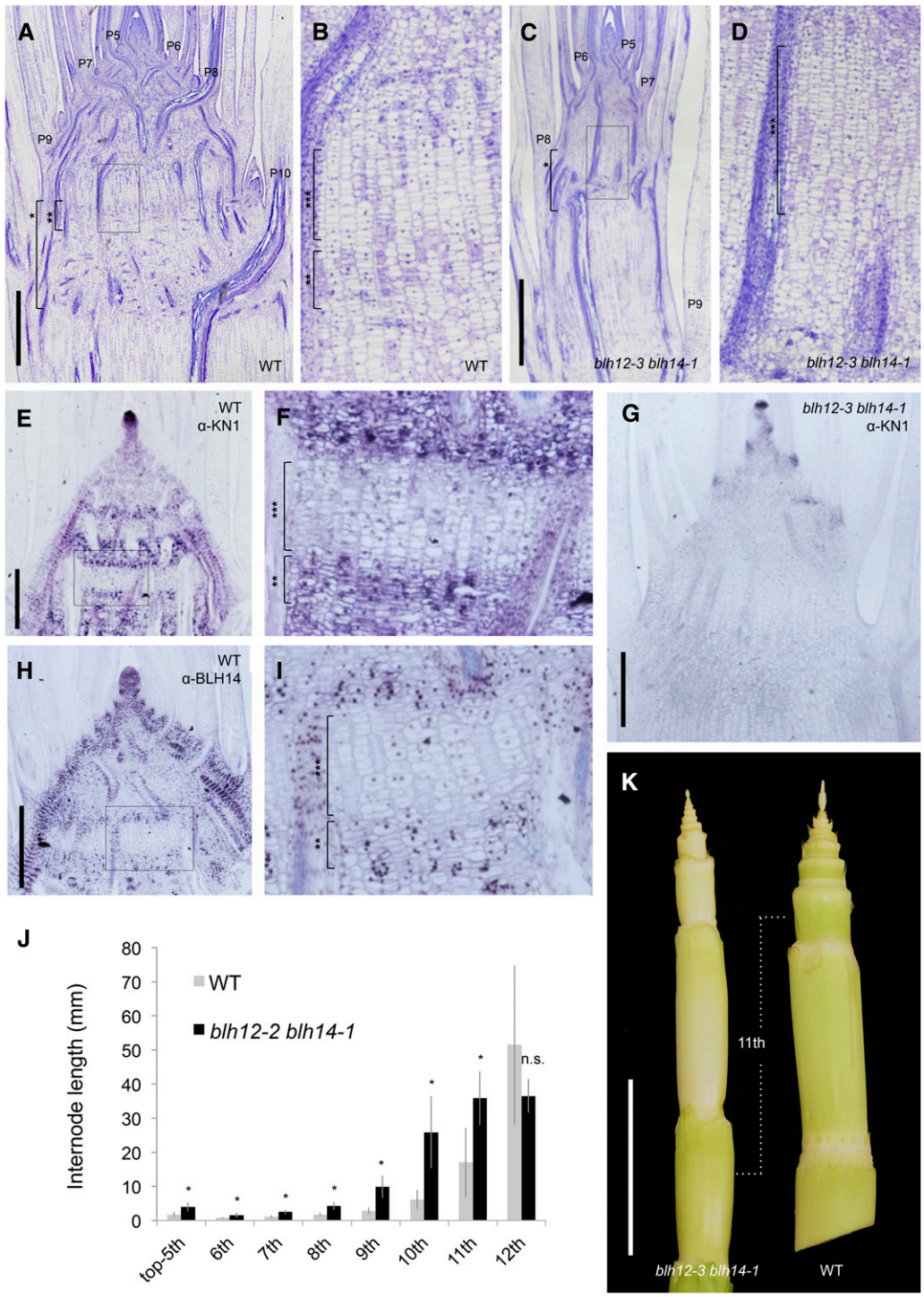

Figure 4. Precocious Differentiation of Internode Results in the Dwarfism in *blh12-3 blh14-1* Mutants.

(A) and **(B)** Tissue sections of wild-type (WT) developing stem at 4 weeks old.
(B) Magnified image of the boxed region in **(A)**.
(C) and **(D)** Tissue sections of *blh12-3 blh14-1* developing stem at 4 weeks old. **(D)** is a magnified image of the boxed region in **(C)**.
(E) and **(F)** KN1 immunostaining in the wild type at 4 weeks old.
(F) Magnified image of the boxed region in **(E)**. KN1-negative cells represent the vertical files of internode cells.
(G) KN1 immunostaining in the *blh12-3 blh14-1* mutant at 4 weeks old.

Abnormal Branching and Delayed Tassel Development in *blh12/14* Double Mutants

Another striking phenotype of *blh12/14* mutants was a highly branched tassel. In the vegetative phase, the SAM in double mutants was mostly normal, although the height was slightly shorter compared with the wild type (Supplemental Figures 7G to 7J). After the transition from vegetative to reproductive development, however, the morphology of the double mutant tassel greatly deviated from the wild type. At 6 weeks, wild-type tassels had several long branches at the base and spikelet meristems on the main axis (Figures 5B and 5D). In comparison, double mutant tassels were much shorter, lacked spikelet meristems, and, instead, initiated numerous branch-like meristems on the main axis (Figures 5C and 5E). At 7 weeks, wild-type tassels were initiating floral organs, whereas *blh12/14* mutant tassels were still branching (Figures 5F and 5G). Although these branch-like meristems expressed KN1, strong accumulation was limited to the tip region (Figure 5H). At 8 weeks, the double mutant had an extremely branched tassel (Figure 5I). Some bract-like bulges initiated on these meristems, indicating initiation of determinate organs (Figure 5I, arrowheads in inset). These results suggest that an indeterminate branching pattern delays normal floral development.

Intriguingly, a week later (9 weeks old), these branch-like meristems shriveled and collapsed. Tassel branches and the rachis kept growing, although their elongation was severely reduced compared with wild-type plants (Figures 3A to 3C, 5J, and 5K).

BLH12 and BLH14 Are Required for Intermediate Vein Formation in Leaves and to Prevent Precocious Anastomosis in the Stem

In the summer field condition, 10 out of 15 *blh12/14* double mutants showed a withered leaf phenotype at 7 weeks old. In these individuals, several upper leaves eventually died (Supplemental Figures 8A and 8B). This phenotype was not observed when double mutants were grown in well-watered condition in the greenhouse (Supplemental Figure 8C), suggesting that it was caused by water deficit. Since water is conducted by veins and BLH12 and BLH14 are strongly expressed in provascular bundles in the young stem, we observed hand sections of mature tassel rachises. We found that the number of veins was severely reduced in the *blh12/14* double mutants, whereas each single mutant had comparable numbers of veins to the wild type (Figures 6A to 6C; Supplemental Figure 8D). Strikingly, most of the reduction in vein number was due to loss of vascular bundles adjacent to the epidermis (defined as outer veins), which decreased to <10% of wild-type numbers (Figure 6D). Vascular bundle number was also significantly lower in the inner stem, by approximately half (Figure 6D). Because *blh12/14* tassel primordia showed an abrupt shriveling during development, we also observed vascular bundles in tassel branches. As in the rachis, *blh12/14* tassel branches had many fewer vascular bundles, especially near the epidermis (Supplemental Figure 9).

To obtain a comprehensive view of vascular bundle defects, we observed stem samples at 6 weeks by micro-CT (computed tomography) scanning. The number of vascular bundles in the *blh12/14* stem was greatly reduced in both the outer and inner regions (Figures 6E and 6F; Supplemental Movie 1). In immature leaves, the number of intermediate veins, but not lateral veins, was severely reduced (Figures 6G to 6J). Reduction of intermediate vein number was also observed in mature leaf blades of double mutants (Supplemental Figure 10).

During leaf development, midveins initiate at P0 to P1, then lateral veins are added as leaf margins grow (P1 or later), and intermediate veins appear between lateral veins at P5 or later (Sharman, 1942). Therefore, BLH12 and BLH14 are important for intermediate vein formation at relatively late stages during leaf development. Consistent with this interpretation, BLH12 and BLH14 accumulate in the abaxial epidermis of P2 to P5 leaves (Figures 6K to 6P), but this expression is transient since it was barely detectable at later stages (Figures 2G and 2I). At leaf insertion points, lateral veins bend inward to the stem center, whereas intermediate veins remain near the epidermis (Supplemental Movie 1) (Esau, 1943). Thus, reduction of intermediate vein formation is likely to be the major cause of the severe vein reduction at the stem periphery.

Intriguingly, we found that lateral veins often anastomosed a few nodes below their leaf insertion points in double mutants. In contrast, lateral veins of the wild type rarely anastomosed with each other and remained independent through several nodes below the leaf insertion point (Figures 7A and 7B; Supplemental Movies 2 and 3). We counted the number of anastomosis events and found that 54 to 78% of veins arriving from leaf laterals precociously fused in the double mutants, whereas only 2 to 9% anastomosed in the wild type ($n = 3$; Figures 7C to 7E; Supplemental Movie 1). Higher order vein fusions were also found in the double mutants (Figure 7E). Serial sections confirmed that provascular bundles anastomosed in the very young stems just beneath the SAM (Supplemental Figure 11 and Supplemental Movies 4 and 5). Collectively, precocious and higher order anastomosis further reduced the number of veins in the double mutants.

Higher magnification of the tassel rachis sections revealed that the double mutant vascular bundles are thicker and have more xylem vessels (Figures 7F and 7G). In the double mutants, 39 to 67% of vascular bundles had three or more xylem vessels (Figure 7H).

Figure 4. (continued).

(H) and **(I)** BLH14 immunostaining in the wild type at 4 weeks old. **(I)** is a magnified image of the boxed region in **(H)**.

(J) Internode length of the wild type and *blh12-3 blh14-1* at 6 weeks old. Internode length is the average of eight plants for each genotype. Asterisks indicate statistically significant differences at $P < 0.01$ compared with the wild type in Student's *t* test. Error bars represent SD.

(K) Stems of *blh12-3 blh14-1* (left) and wild type (right) at 7 weeks old.

Bars = 1 mm in **(A)** and **(C)**, 500 μm in **(E)**, **(G)**, and **(H)**, and 4 cm in **(K)**. Brackets with single, double, and triple asterisks represent nodes, putative intercalary meristems, and internodes, respectively.

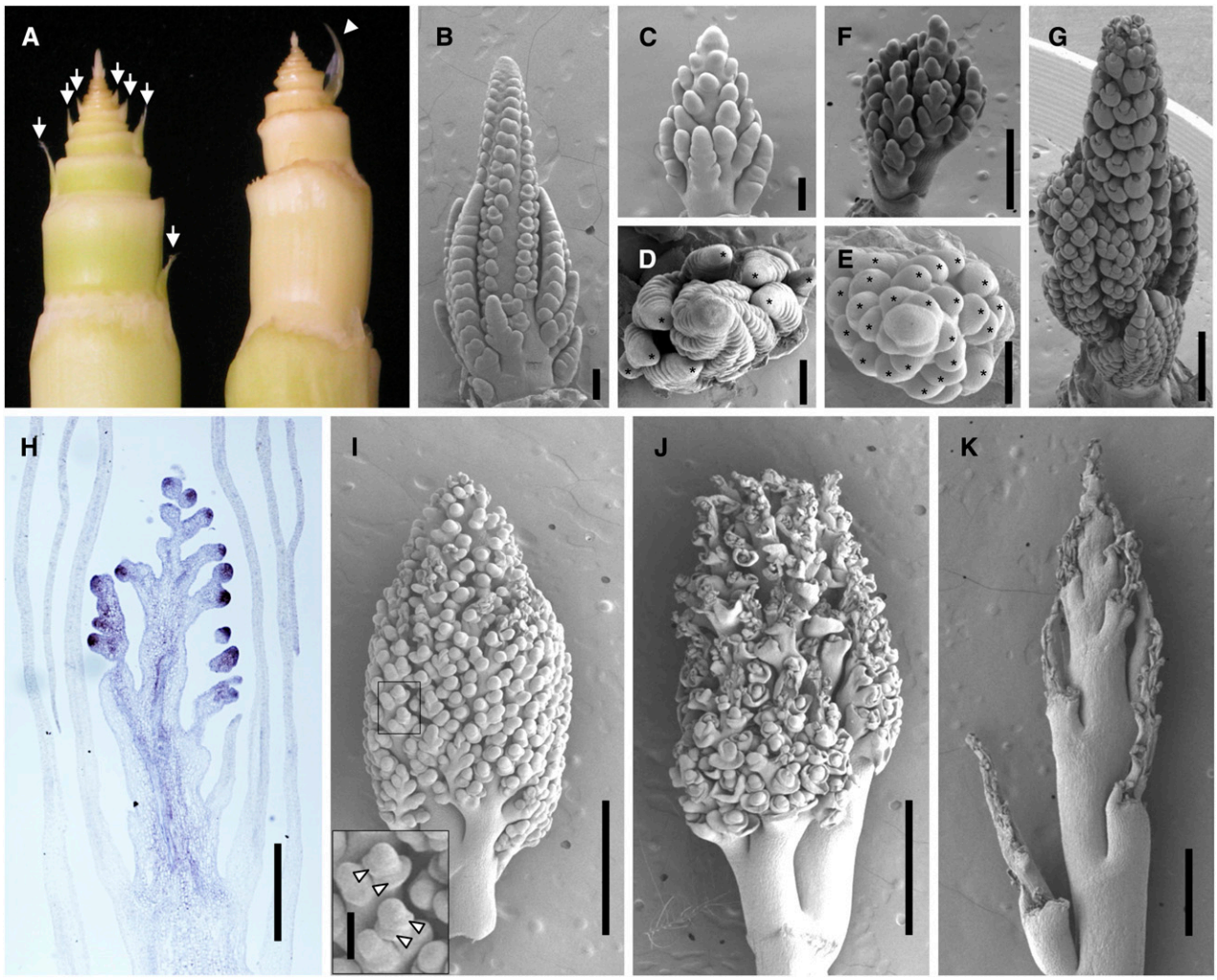

Figure 5. *blh12-3 blh14-1* Phenotypes during Tassel Development.

(A) Wild-type (left) and *blh12-3 blh14-1* (right) shoot apices at 6 weeks old. Arrows and an arrowhead indicate axillary buds and an empty prophyll occasionally formed, respectively. Tassels can be seen at apices.
(B) Wild-type tassel at 6 weeks old.
(C) *blh12-3 blh14-1* tassel at 6 weeks old.
(D) Top view of **(B)**.
(E) Top view of **(C)**.
(F) *blh12-3 blh14-1* tassel at 7 weeks old.
(G) Wild-type tassel at 7 weeks old.
(H) KN1 immunostaining in the *blh12-3 blh14-1* tassel at 6 weeks old.
(I) to **(K)** *blh12-3 blh14-1* tassel at 8 **(I)**, 9 **(J)**, and 10 **(K)** weeks old. A box indicates the magnified area shown in the inset. Arrowheads indicate bract-like bulges.
Bars = 200 μm in **(B)** to **(E)**, 500 μm in **(F)** to **(H)**, 1 mm in **(I)** to **(K)**, and 100 μm in the inset in **(I)**.

In an extreme case, six xylem vessels were observed in a single vascular bundle. In contrast, most wild-type vascular bundles possessed two xylem vessels, or three at a maximum. Thus, the excess anastomosis is likely to result in thicker veins with increased vessels.

Polar transport of the phytohormone auxin from leaf primordia into the stem guides the position of vascular traces (Bayer et al., 2009). The transport of auxin is performed by auxin export proteins called PIN-FORMED1 (PIN1) (Gälweiler et al., 1998). Classic experiments performed by Sachs showed that a local application of auxin on the cut surface of a stem induces the formation of new veins and that existing veins attract such new vascular strands unless the existing vein is also given an auxin application (Sachs, 1968). Given these experiments, we tested whether expression of maize PIN1a was maintained in *blh12/14* veins undergoing fusion.

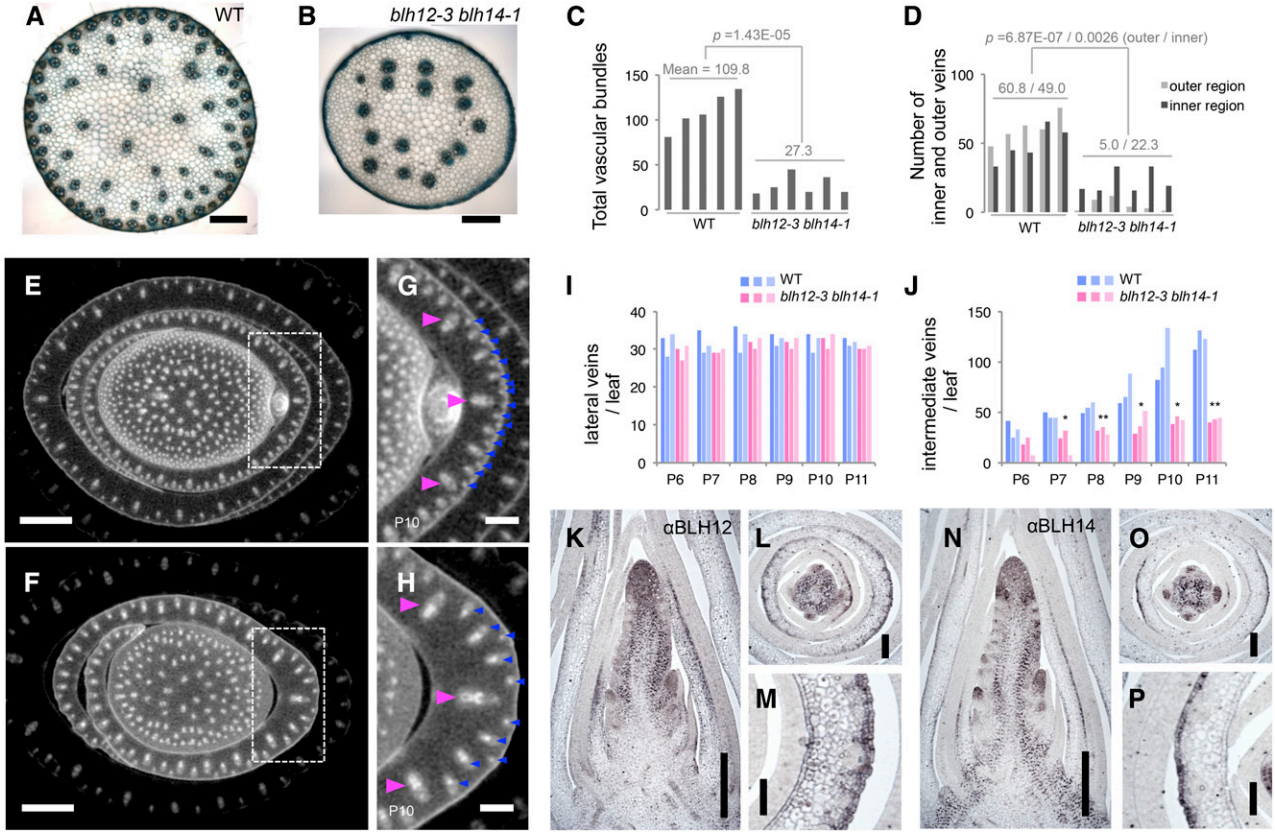

Figure 6. *blh12-3 blh14-1* Double Mutants Had Fewer Vascular Bundles in Stems and Leaves.

(A) and **(B)** Transverse hand sections of wild-type (WT; **[A]**) and *blh12-3 blh14-1* **(B)** tassel rachis.
(C) Measurement of total numbers of vascular bundles in the tassel rachis.
(D) Measurement of vascular bundles in inner and outer regions of the tassel rachis. Vein numbers were counted in five and six individuals in the wild type and *blh12-3 blh14-1*, respectively. Mean values and P values in Student's *t* test are represented in **(C)** and **(D)**. The "E" in the P value represents "exponent."
(E) to **(H)** Micro-CT scanning images of wild-type (**[E]** and **[G]**) and *blh12-3 blh14-1* (**[F]** and **[H]**) stems. **(G)** and **(H)** are magnified images indicated with dashed boxes in **(E)** and **(F)**, respectively. Lateral and intermediate veins in the P10 leaf primordium are marked with magenta and blue arrowheads, respectively.
(I) and **(J)** Number of lateral **(I)** and intermediate **(J)** veins in the wild type (blue) and *blh12-3 blh14-1* (magenta). Vein numbers were counted in three individuals in each genotype. Single and double asterisks represent significant difference between the wild type and *blh12-3 blh14-1* in Student's *t* test at $P < 0.05$ and < 0.01, respectively.
(K) to **(P)** Immunostaining for BLH12 (**[K]** to **[M]**) and for BLH14 (**[N]** to **[P]**) in wild-type shoot apices at 5 weeks old, showing protein accumulation in the abaxial epidermis and a few inner cell layers of developing leaves.
Bars = 500 μm in **(A)**, **(B)**, **(G)**, **(H)**, **(K)**, and **(N)**, 2 mm in **(E)** and **(F)**, 200 μm in **(L)** and **(O)**, and 100 μm in **(M)** and **(P)**.

Fused veins in *blh12/14* mutants still express PIN1a, indicating that the defects causing precocious anastomosis were not likely due to PIN1a (Supplemental Movies 6 and 7).

We analyzed vascular BLH14 accumulation in developing stems by immunolocalization. From the SAM to P4 leaf insertion, BLH14 was expressed in the entire stem (Figures 7I and 7J). At the P5 leaf insertion, BLH14 accumulation decreased in the central parenchyma and in the lateral veins arriving from the P5 leaf primordium (Figure 7K). At the same time, strong BLH14 expression was detected in young provascular bundles. Interestingly, BLH14 was initially expressed throughout provascular bundles, but adopted a ring-shaped expression pattern in older provascular strands (Figure 7L). Thus, the BLH14 expression domain coincided not only with the young stem region where vascular bundles differentiate, but also with the developing provascular bundle itself. Given the vein fusions in *blh12/14* mutants, this dynamic expression pattern is likely required for preventing vein fusions.

DISCUSSION

BLH12 and BLH14 are KN1 cofactors that have overlapping protein accumulation domains. To investigate possible redundancy with KN1 function, we obtained loss-of-function mutants and analyzed the double mutant phenotype. Some phenotypes are reminiscent of *KNOX* loss of function, but others are unique, revealing novel roles for these TALE TFs. Most strikingly, BLH12 and

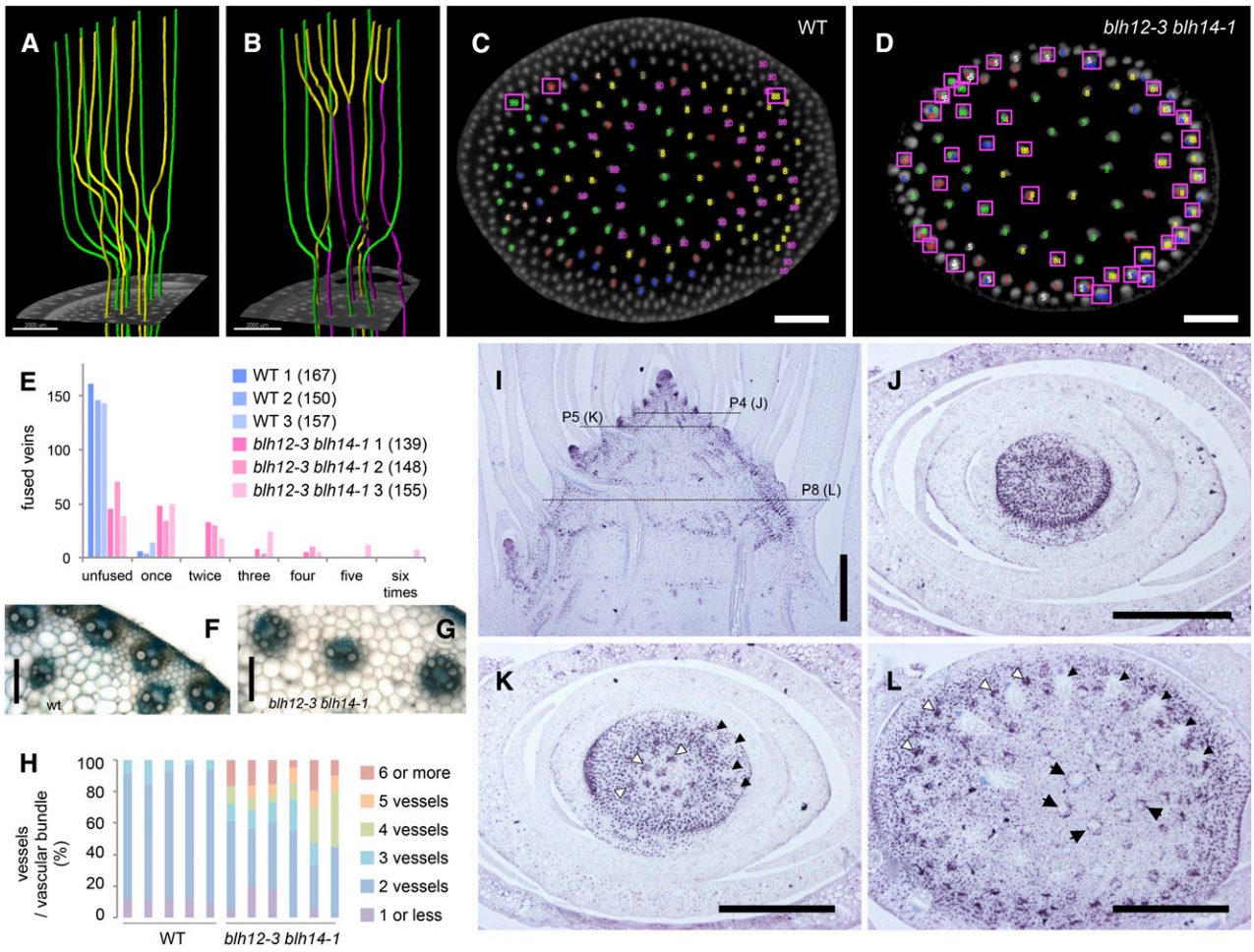

Figure 7. Precocious Vein Anastomosis in *blh12-3 blh14-1* Stems and BLH14 Expression Patterns in the Wild Type.

(A) and **(B)** 3D images of vein traces extracted from micro-CT data showing anastomosed veins (magenta) occurring in the double mutant **(B)** but not in the wild type **(A)**. Veins are colored according to leaf of origin in green and yellow.

(C) and **(D)** Veins arriving from leaf laterals are traced downwards in micro-CT data (Supplemental Movie 1) and mapped in the cross sections of the tenth and ninth internodes in the wild type **(C)** and *blh12-3 blh14-1* double mutants **(D)**, respectively. Anastomosed veins are indicated with magenta boxes. Veins arriving from the same leaf are marked in one color.

(E) Counts of anastomosed veins. Veins are classified by number of anastomosis events. Anastomosis events were counted in three individuals in each genotype. The number in the parentheses indicate the total number of veins observed.

(F) and **(G)** Vascular bundles in wild-type **(F)** and *blh12-3 blh14-1* **(G)** tassel rachises.

(H) Measurement of xylem vessel numbers per vascular bundle in tassel rachises. Five and six individuals were observed in the wild type and *blh12-3 blh14-1*, respectively.

(I) to **(L)** BLH14 immunostaining in the wild-type stem. Dashed lines in the vertical section **(I)** indicate the levels of cross sections below P4, P5, and P8 leaf insertion points in **(J)** to **(L)**, respectively. White arrowheads indicate young provascular bundles that accumulate BLH14 in entire diameter. Black arrows are older provascular bundles with BLH14 accumulation in the ring-shaped pattern. Black arrowheads show older veins in which BLH14 is downregulated. Bars = 2 mm in **(A)** to **(D)**, 100 μm in **(F)** and **(G)**, and 500 μm in **(I)** to **(L)**.

BLH14 are needed to initiate intermediate veins in the leaf and prevent anastomosis of lateral veins in the stem.

BLH12 and BLH14 Promote Determinacy and Developmental Progression of Shoot Meristems

blh12/14 double mutants show contrasting defects in lateral organ initiation dependent on developmental context. During vegetative growth, the SAM was properly maintained and produced a normal number of leaves, although SAM height was slightly shorter than the wild type. Axillary meristems, in contrast, were not maintained, resulting in a lack of tillers and ears. These meristem defects are reminiscent of *kn1* loss-of-function alleles (Kerstetter et al., 1997; Vollbrecht et al., 2000). In Arabidopsis, the SAM of *pny pnf* double mutants frequently terminates but organogenesis continues from leaf axils (Rutjens et al., 2009; Ung et al., 2011; Khan et al., 2015).

The triple mutant with a third *BLH* gene, *ath1*, results in failure in SAM establishment during embryogenesis (Rutjens et al., 2009). Therefore, other maize BLH proteins could act with KNOX proteins in SAM maintenance and establishment. The failure of axillary meristem maintenance in *blh12/14* and high level of accumulation of BLH12 and BLH14 in these tissues suggest that these two BLHs in the PNY clade have essential functions in axillary meristem maintenance as KNOX cofactors.

The *blh12/14* terminal inflorescence (tassel) showed an unexpected phenotype. In wild-type tassels, axillary meristems along the tassel branches and main rachis progress to become determinate spikelet meristems. *kn1* loss-of-function mutants make fewer branches and fewer spikelets (Kerstetter et al., 1997). By contrast, *blh12/14* inflorescences continue to make indeterminate branches, delaying spikelet meristem initiation. This indeterminate phenotype is reminiscent of *ramosa1* (*ra1*) mutants, except *ra1* tassels are fertile. RA1 is known to impose determinacy, and heterochrony of *ra1* expression was implicated in the diverse inflorescence architecture of grasses (Vollbrecht et al., 2005). Interestingly, the highly branched tassels in *blh12/14* resembled those of sorghum (*Sorghum bicolor*), in which inflorescence meristems produce indeterminate branches initially and delay acquisition of determinate spikelet pair fate. Genome-wide studies show that RA1 and KN1 share many direct targets (Bolduc et al., 2012; Eveland et al., 2014). It is possible that BLHs also share downstream targets with RA1 to promote determinacy, antagonistic to KN1, which promotes meristem fate.

An alternative explanation is that *blh12/14* fail to progress to flowering, similar to the double mutant of Arabidopsis homologs, *pny pnf*, which never produce flowers and do not express floral meristem identity genes (Smith et al., 2004). Indeed, induction of flowering by overexpression of *FLOWERING LOCUS T* is suppressed in *pny pnf* (Kanrar et al., 2008). One difference between *pny pnf* and *blh12/14* double mutants is that the former fails to transition to flowering, whereas *blh12/14* mutants have become reproductive, they just fail to make flowers, possibly due to the vascular defect.

Function of BLH12 and BLH14 in Node and Internode Development

Phytomers are the repeating unit of plant development, consisting of a node to which a leaf is attached, a subtending internode, and an axillary bud at the base of the leaf. Together, the internodes and nodes comprise the stem, important for moving solutes through the plant and providing mechanical support. *blh12/14* mutants have a unique internode phenotype. Internodes elongate precociously, but then fail to maintain their ability to elongate. An internode phenotype was also noted in the loss-of-function mutants of a rice *KNOX* gene, *Oryza sativa homeobox 15* (*OSH15*), which shows a dwarf phenotype due to failure of internode elongation (Sato et al., 1999). Consistent with this finding, double mutants of *kn1* and another maize *KNOX* gene, *rough sheath1*, are shorter if they are not well introgressed into B73 (Bolduc et al., 2014). Thus, these reports suggest that KNOX proteins are likely to have similar functions with BLH12/14 in stem development as cofactors. In Arabidopsis, mutations in *PNY* also cause severely shortened internodes, resulting in clustered siliques (Smith and Hake, 2003). Detailed analysis suggests the defect in *pny* is due to cell division orientation rather than cell proliferation (Bencivenga et al., 2016). Mutations in organ boundary genes restore the *pny* internode defect (Khan et al., 2015; Bencivenga et al., 2016). Thus, both maize and Arabidopsis putative orthologs play a role in internode elongation, but possibly through different mechanisms due to the differences in growth habit.

We found that KNOX and BLH proteins accumulate in a horizontal zone of mitotically active cells, the presumed intercalary meristem, prior to differentiation and elongation of the internode. Above this zone are vertical cell files of internodal parenchyma, in which both KNOX and BLH are downregulated. In *blh12/14* mutants, these internodal cell files precociously differentiate and the intercalary meristem is lost. These results suggest that the intercalary meristem, which produces the internode parenchyma cells, is maintained by BLH proteins.

The reticulated network of horizontal veins is reduced in *blh12/14* mutant nodes (Supplemental Movies 1 to 3). This reduction likely results from the lack of axillary meristems that would normally produce numerous veins from the husk leaves. It is also possible that BLHs and KN1 expressed in nodes have a direct role in forming further reticulated networks. Mineral transporters are expressed in nodes of grass species; therefore, nodal veins have important functions for the distribution of mineral elements (Yamaji and Ma, 2014). Because developing tissues such as shoot apices are low in transpiration but high in nutrient requirements, the intervascular exchange of mineral elements through the nodal vein network is particularly important.

Regulation of Vein Formation and Anastomosis

A defining monocot feature is parallel venation in leaves and scattered veins in stems. As lateral veins enter the stem, they bend toward the center, whereas intermediate veins run downwards at the stem periphery (Supplemental Movie 1). In maize, lateral veins remain independent through several nodes below their leaf insertion point with a gradual shift toward the stem periphery. Therefore, the small veins at the periphery are a mixture of lateral and intermediate veins, whereas large veins at the center of the stem are only laterals. In nodes, the small veins at the periphery often branch to form a reticulate network or anastomose to each other. Thus, in monocots that lack a vascular cambium, the number of veins initiated in leaves directly contributes to that in the mature stem. Given the water deficit phenotype of *blh12/14*, initiation of many independent veins must be crucial for maize to meet water demand as plants mature.

blh12/14 mutants initiate fewer intermediate veins in the leaf and thus have a drastic reduction in veins at the periphery of the stem. BLH12 and BLH14 accumulate on the abaxial side of a developing leaf in a transient fashion, consistent with the timing of intermediate vein initiation. Given that KN1 is not expressed in leaves, other KNOX cofactors may regulate intermediate vein formation in leaves. *liguleless3*, which is expressed in developing leaves (Johnston et al., 2014), is a reasonable candidate to interact with BLH12 and BLH14.

Given the reticulate venation found in most vascular plants, and indeed in certain regions of the maize plant, it is impressive that lateral veins differentiate near each other in the maize stem without fusion. Our data show that anastomosis is prevented by BLH12 and BLH14. Just below the SAM, BLHs are expressed throughout the stem but are restricted to outer regions at lower and more

differentiated regions of the stem. This BLH expression domain corresponds with the area in which lateral veins remain independent. Once veins mature and BLH12/14 are downregulated, anastomosis may occur between the other veins.

Classical experiments performed by Sachs, as well as a large body of recent studies, have shown that auxin flow determines vascular traces (Sachs, 1981; Bennett et al., 2014). Although the accumulation of PIN1a was not altered, PIN1b, another PIN1 protein broadly expressed in the stem, is thought to have a role in determining future vein traces (O'Connor et al., 2014). Chromatin immunoprecipitation-sequencing studies showed that KNOX proteins directly bind loci involved in multiple levels of auxin regulation (Bolduc et al., 2012; Tsuda et al., 2014). Further studies should determine the relationship between auxin, BLHs, and anastomosis.

METHODS

Plant Materials

All mutant alleles were isolated from *Mu* transposon-mutagenized populations and identified using *Mu*-end primers and either *blh12* or *blh14* primers. Primers used for genotyping are listed in Supplemental Table 2. Mutant alleles were introgressed into B73 by backcrossing at least three times. Plants were grown in the field at Albany, CA.

Phylogenic Analysis

Amino acid sequences for maize (*Zea mays*) and *Arabidopsis thaliana* BLH proteins were obtained by BLAST searching in MaizeGDB and TAIR, respectively. Gene IDs are listed in Supplemental Table 3. Full-length amino acid sequences were aligned using ClustalW (www.genome.jp/tools/clustalw/). The phylogenic relationship was inferred using the maximum likelihood method implemented in RAxML (Stamatakis, 2014) with the JTT substitution model, and the maximum likelihood tree was evaluated with 1000 bootstrap replicates.

BiFC Assay

Coding regions of *blh12* and *blh14* were amplified using primers listed in Supplemental Table 2, cloned into the pENTR vector (Invitrogen), and transferred to BiFC vectors pB7WGYN2 or pB7WGYC2. These BiFC constructs were introduced into *Agrobacterium tumefaciens* strain GV3101. Agroinfiltration into *Nicotiana benthamiana* leaves was performed as described previously (Bolduc and Hake, 2009). Two to three days later, infiltrated leaves were observed under LSM710 confocal microscopy (Zeiss) with 470-nm excitation and 535-nm emission filters. Nuclei were stained with 4′,6-diamidino-2-phenylindole.

Antibody Production

Full-length BLH12 and BLH14 coding regions were cloned into pDEST17 and pDEST15 expression vectors (Invitrogen) for antigen production and affinity purification, respectively. Antibody production in guinea pigs and affinity purification were performed as previously described (Chuck et al., 2014).

Coimmunoprecipitation

Total protein was extracted by grinding 4 g of pooled maize shoot apices (1 cm in length) in liquid nitrogen. The resulting powder was resuspended in twice the volume of extraction buffer containing 50 mM Tris (pH 7.5), 150 mM NaCl, 1.5% IGEPAL-CA-630 (Sigma-Aldrich), and 1× protease inhibitor mix (Roche), filtered through four layers of Miracloth, and centrifuged at 4000*g* for 10 min at 4°C. Protein extract was incubated with 25 μL Protein A magnetic beads coupled to polyclonal anti-BLH12 or BLH14 antibody for 45 min at 4°C. Magnetic bead-bound target protein was magnetically separated and washed four times with 200 μL ice-cold wash buffer containing 50 mM Tris (pH 7.5), 150 mM NaCl, 0.1% IGEPAL-CA-630 (Sigma-Aldrich), and 1× protease inhibitor mix (Roche). Bound target proteins were eluted twice with 100 μL of elution buffer (0.2% SDS, 0.1% Tween 20, and 50 mM Tris-HCl, pH 7.5). Eluted proteins were precipitated with acetone and pellets were resuspended in 1× SDS-PAGE loading buffer. Following standard SDS-PAGE electrophoresis and immunoblotting, coimmunoprecipitated BLH proteins were detected using chemiluminescence with anti-BLH12 or anti-BLH14 antibody and a secondary HRP-coupled anti-guinea pig IgG antibody (sc-2438; Santa Cruz Biotechnology). KN1 protein was detected in BLH coimmunoprecipitation using anti-KN1 antibody and secondary HRP-coupled anti-rabbit IgG antibody. Coimmunoprecipitation experiments were performed with three biological replicates.

Histological Analyses and Immunohistochemistry

Standard paraffin sections were prepared as previously described (Tsuda et al., 2011). For histological observations, tissue sections were stained with toluidine blue. Hand sections of tassel rachis were stained with toluidine blue and washed in 20% acetic acid. Immunostaining was performed as previously described (Chuck et al., 2010) except for the epitope retrieval by heating 10-μm paraffin sections in a microwave in a sodium citrate buffer (10 mM sodium citrate and 0.05% Tween 20, pH 6.0) for 10 min.

Scanning Electron Microscopy

Maize young tassels were fixed, sputter-coated, and observed on a Hitachi S-4700 scanning electron microscope at an accelerating voltage of 5 kV as previously described (Tsuda et al., 2014).

Micro-CT Scanning

Stem samples were harvested from 6-week-old plants and fixed in FAA fixative solution (formalin:acetic acid:50% ethanol = 5:5:90) for a week. Fixative was replaced with 70% ethanol and stored at 4°C until observation. Before scanning, maize tissues were soaked in contrast agent, a 0.3% phosphotungstic acid in 70% ethanol solution, or a 1:3 mixture of Lugol's solution and deionized distilled water, as previously described (Metscher, 2009; Staedler et al., 2013; Degenhardt et al., 2010). Maize tissues were scanned using x-ray micro-CT at a tube voltage peak of 80 kVp and a tube current of 90 μA. Samples were rotated 360° in steps of 0.18°, generating 2000 projection images of 992 × 992 pixels. The micro-CT data were reconstructed at an isotropic resolution of 9.4 × 9.4 × 9.4 μm^3. Three-dimensional, tomographic images were obtained using the OsiriX software program. Vein traces were extracted from the micro-CT data using Imaris 8.2 and FilamentTracer (http://www.bitplane.com/imaris-for-neuroscientists).

Accession Numbers

Accession numbers of ZmBLH12, ZmBLH13, and ZmBLH14 amino acid sequences are DAA56836.1, AFW81703.1, and AFW78222.1, respectively. Other accession numbers and gene IDs used in the phylogenic analysis are listed in Supplemental Table 3.

Supplemental Data

Supplemental Figure 1. Relative expression levels of BLH genes in various tissues.

Supplemental Figure 2. Accumulation patterns of BLH12 and BLH14 in wild type.

Supplemental Figure 3. Measurement of plant height and leaf number in blh12/14 mutants.

Supplemental Figure 4. Double mutant phenotypes during vegetative growth.

Supplemental Figure 5. Tissue sections of stems at 4 weeks old.

Supplemental Figure 6. Immunostaining of BLH12 in the young stem.

Supplemental Figure 7. Phenotypes of *blh12-3 blh14-1* vegetative shoot apices.

Supplemental Figure 8. Leaf drought phenotype of *blh12-3 blh14-1* grown in summer field conditions.

Supplemental Figure 9. Fewer vascular bundles form in *blh12-3 blh14-1* tassel branches.

Supplemental Figure 10. Transverse sections of leaf blades formed below tassels.

Supplemental Figure 11. Veins precociously fuse just below the SAM in *blh12-3 blh14-1*.

Supplemental Table 1. Numbers of individuals that produced tillers in the family segregating *blh12-2 blh14-1* double mutants.

Supplemental Table 2. Oligo DNA sequences.

Supplemental Table 3. Gene IDs and accession numbers.

Supplemental Movie 1. Micro-CT scans along the longitudinal axis of stems containing from tassel to P10 leaves at 6 weeks old.

Supplemental Movie 2. A micro-CT scan along the longitudinal axis in wild-type 10th node from the apex at 6 weeks old.

Supplemental Movie 3. A micro-CT scan along the longitudinal axis in *blh12-3 blh14-1* 10th node from the apex at 6 weeks old.

Supplemental Movie 4. Horizontal sections of the wild-type shoot apex at 4 weeks old.

Supplemental Movie 5. Horizontal sections of the *blh12-3 blh14-1* shoot apex at 4 weeks old.

Supplemental Movie 6. PIN1a immunolocalizations in the wild-type shoot apex at 4 weeks old.

Supplemental Movie 7. PIN1a immunolocalizations in the *blh12-3 blh14-1* shoot apex at 4 weeks old.

Supplemental Movie Legends.

Supplemental File 1. Amino acid sequence alignments of BLH proteins used to generate the phylogenic tree.

ACKNOWLEDGMENTS

We thank Jennifer Lewis for providing BiFC vectors and Lia Poasi for taking care of maize plants in our greenhouse. We also thank all Hake lab members for supporting this work and for critically reading the manuscript. This work was supported by JSPS KAKENHI Grant JP16K18637 to K.T., NSF PGRP-1339332 to Z.D., and NSF DEB-1457023 to S.H.

AUTHOR CONTRIBUTIONS

K.T. and S.H. designed this work. K.T. performed all experiments except for protein coimmunoprecipitation. M.-J.A.-J. contributed to mutant phenotype observations and conducted protein coimmunoprecipitation as well as the BiFC assay during manuscript revision. A.M. and K.T. obtained micro-CT scanning data. Z.D. contributed to sample preparation for micro-CT scanning. D.A. contributed to the production of anti-BLH14 antibody and BiFC constructs. R.M. produced *Mu* insertion lines. K.T., M.-J.A.-J., T.S., K.N., and S.H. analyzed the data. K.T. and S.H. wrote the manuscript.

Received December 28, 2016; revised March 3, 2017; accepted March 28, 2017; published April 5, 2017.

REFERENCES

Bayer, E.M., Smith, R.S., Mandel, T., Nakayama, N., Sauer, M., Prusinkiewicz, P., and Kuhlemeier, C. (2009). Integration of transport-based models for phyllotaxis and midvein formation. Genes Dev. **23:** 373–384.

Bencivenga, S., Serrano-Mislata, A., Bush, M., Fox, S., and Sablowski, R. (2016). Control of oriented tissue growth through repression of organ boundary genes promotes stem morphogenesis. Dev. Cell **39:** 198–208.

Bennett, T., Hines, G., and Leyser, O. (2014). Canalization: what the flux? Trends Genet. **30:** 41–48.

Bhatt, A.M., Etchells, J.P., Canales, C., Lagodienko, A., and Dickinson, H. (2004). VAAMANA–a BEL1-like homeodomain protein, interacts with KNOX proteins BP and STM and regulates inflorescence stem growth in *Arabidopsis.* Gene **328:** 103–111.

Bolduc, N., and Hake, S. (2009). The maize transcription factor KNOTTED1 directly regulates the gibberellin catabolism gene *ga2ox1.* Plant Cell **21:** 1647–1658.

Bolduc, N., Tyers, R.G., Freeling, M., and Hake, S. (2014). Unequal redundancy in maize knotted1 homeobox genes. Plant Physiol. **164:** 229–238.

Bolduc, N., Yilmaz, A., Mejia-Guerra, M.K., Morohashi, K., O'Connor, D., Grotewold, E., and Hake, S. (2012). Unraveling the KNOTTED1 regulatory network in maize meristems. Genes Dev. **26:** 1685–1690.

Bürglin, T.R., and Affolter, M. (2016). Homeodomain proteins: an update. Chromosoma **125:** 497–521.

Byrne, M.E., Groover, A.T., Fontana, J.R., and Martienssen, R.A. (2003). Phyllotactic pattern and stem cell fate are determined by the Arabidopsis homeobox gene *BELLRINGER.* Development **130:** 3941–3950.

Chuck, G., Whipple, C., Jackson, D., and Hake, S. (2010). The maize SBP-box transcription factor encoded by tasselsheath4 regulates bract development and the establishment of meristem boundaries. Development **137:** 1243–1250.

Chuck, G.S., Brown, P.J., Meeley, R., and Hake, S. (2014). Maize SBP-box transcription factors unbranched2 and unbranched3 affect yield traits by regulating the rate of lateral primordia initiation. Proc. Natl. Acad. Sci. USA **111:** 18775–18780.

Degenhardt, K., Wright, A.C., Horng, D., Padmanabhan, A., and Epstein, J.A. (2010). Rapid 3D phenotyping of cardiovascular development in mouse embryos by micro-CT with iodine staining. Circ Cardiovasc Imaging **3:** 314–322.

Esau, K. (1943). Ontogeny of the vascular bundle in *Zea mays*. Hilgardia **15:** 327–368.

Eveland, A.L., et al. (2014). Regulatory modules controlling maize inflorescence architecture. Genome Res. **24:** 431–443.

Gälweiler, L., Guan, C., Müller, A., Wisman, E., Mendgen, K., Yephremov, A., and Palme, K. (1998). Regulation of polar auxin transport by AtPIN1 in Arabidopsis vascular tissue. Science **282:** 2226–2230.

Hedden, P. (2003). The genes of the Green Revolution. Trends Genet. **19:** 5–9.

Jackson, D., Veit, B., and Hake, S. (1994). Expression of maize *KNOTTED1* related homeobox genes in the shoot apical meristem predicts patterns of morphogenesis in the vegetative shoot. Development **120:** 405–413.

Johnston, R., Wang, M., Sun, Q., Sylvester, A.W., Hake, S., and Scanlon, M.J. (2014). Transcriptomic analyses indicate that maize ligule development recapitulates gene expression patterns that occur during lateral organ initiation. Plant Cell **26:** 4718–4732.

Johri, M.M., and Coe, E.H., Jr. (1983). Clonal analysis of corn plant development. I. The development of the tassel and the ear shoot. Dev. Biol. **97:** 154–172.

Kanrar, S., Bhattacharya, M., Arthur, B., Courtier, J., and Smith, H.M. (2008). Regulatory networks that function to specify flower meristems require the function of homeobox genes PENNYWISE and POUND-FOOLISH in Arabidopsis. Plant J. **54:** 924–937.

Kaplan, D.R. (2000). Principles of Plant Morphology, Vol. II. (Berkeley, CA: Odin Readers).

Kerstetter, R.A., Laudencia-Chingcuanco, D., Smith, L.G., and Hake, S. (1997). Loss-of-function mutations in the maize homeobox gene, *knotted1*, are defective in shoot meristem maintenance. Development **124:** 3045–3054.

Khan, M., et al. (2015). Repression of lateral organ boundary genes by PENNYWISE and POUND-FOOLISH is essential for meristem maintenance and flowering in Arabidopsis. Plant Physiol. **169:** 2166–2186.

Kumar, R., Kushalappa, K., Godt, D., Pidkowich, M.S., Pastorelli, S., Hepworth, S.R., and Haughn, G.W. (2007). The Arabidopsis BEL1-LIKE HOMEODOMAIN proteins SAW1 and SAW2 act redundantly to regulate KNOX expression spatially in leaf margins. Plant Cell **19:** 2719–2735.

Lee, J.H., Lin, H., Joo, S., and Goodenough, U. (2008). Early sexual origins of homeoprotein heterodimerization and evolution of the plant KNOX/BELL family. Cell **133:** 829–840.

Metscher, B.D. (2009). MicroCT for comparative morphology: simple staining methods allow high-contrast 3D imaging of diverse non-mineralized animal tissues. BMC Physiol. **9:** 11.

O'Connor, D.L., Runions, A., Sluis, A., Bragg, J., Vogel, J.P., Prusinkiewicz, P., and Hake, S. (2014). A division in PIN-mediated auxin patterning during organ initiation in grasses. PLOS Comput. Biol. **10:** e1003447.

Reiser, L., Modrusan, Z., Margossian, L., Samach, A., Ohad, N., Haughn, G.W., and Fischer, R.L. (1995). The *BELL1* gene encodes a homeodomain protein involved in pattern formation in the Arabidopsis ovule primordium. Cell **83:** 735–742.

Roeder, A.H., Ferrándiz, C., and Yanofsky, M.F. (2003). The role of the REPLUMLESS homeodomain protein in patterning the Arabidopsis fruit. Curr. Biol. **13:** 1630–1635.

Rutjens, B., Bao, D., van Eck-Stouten, E., Brand, M., Smeekens, S., and Proveniers, M. (2009). Shoot apical meristem function in Arabidopsis requires the combined activities of three BEL1-like homeodomain proteins. Plant J. **58:** 641–654.

Sachs, T. (1968). On the determination of the pattern of vascular tissue. Ann. Bot. (Lond.) **32:** 781–790.

Sachs, T. (1981). The control of patterned differentiation of vascular tissues. Adv. Bot. Res. **9:** 151–262.

Sanchez, P., Nehlin, L., and Greb, T. (2012). From thin to thick: major transitions during stem development. Trends Plant Sci. **17:** 113–121.

Sato, Y., Sentoku, N., Miura, Y., Hirochika, H., Kitano, H., and Matsuoka, M. (1999). Loss-of-function mutations in the rice homeobox gene *OSH15* affect the architecture of internodes resulting in dwarf plants. EMBO J. **18:** 992–1002.

Sharman, B.C. (1942). Developmental anatomy of the shoot of *Zea mays* L. Ann. Bot. (Lond.) **6:** 245–282.

Smith, H.M.S., Campbell, B.C., and Hake, S. (2004). Competence to respond to floral inductive signals requires the homeobox genes *PENNYWISE* and *POUND-FOOLISH*. Curr. Biol. **14:** 812–817.

Smith, H.M.S., and Hake, S. (2003). The interaction of two homeobox genes, BREVIPEDICELLUS and PENNYWISE, regulates internode patterning in the Arabidopsis inflorescence. Plant Cell **15:** 1717–1727.

Smith, L.G., Greene, B., Veit, B., and Hake, S. (1992). A dominant mutation in the maize homeobox gene, *Knotted-1*, causes its ectopic expression in leaf cells with altered fates. Development **116:** 21–30.

Staedler, Y.M., Masson, D., and Schönenberger, J. (2013). Plant tissues in 3D via X-ray tomography: simple contrasting methods allow high resolution imaging. PLoS One **8:** e75295.

Stamatakis, A. (2014). RAxML version 8: a tool for phylogenetic analysis and post-analysis of large phylogenies. Bioinformatics **30:** 1312–1313.

Tsuda, K., and Hake, S. (2015). Diverse functions of KNOX transcription factors in the diploid body plan of plants. Curr. Opin. Plant Biol. **27:** 91–96.

Tsuda, K., Ito, Y., Sato, Y., and Kurata, N. (2011). Positive autoregulation of a KNOX gene is essential for shoot apical meristem maintenance in rice. Plant Cell **23:** 4368–4381.

Tsuda, K., Kurata, N., Ohyanagi, H., and Hake, S. (2014). Genome-wide study of KNOX regulatory network reveals brassinosteroid catabolic genes important for shoot meristem function in rice. Plant Cell **26:** 3488–3500.

Ung, N., Lal, S., and Smith, H.M. (2011). The role of PENNYWISE and POUND-FOOLISH in the maintenance of the shoot apical meristem in Arabidopsis. Plant Physiol. **156:** 605–614.

Vollbrecht, E., Reiser, L., and Hake, S. (2000). Shoot meristem size is dependent on inbred background and presence of the maize homeobox gene, *knotted1.* Development **127:** 3161–3172.

Vollbrecht, E., Springer, P.S., Goh, L., Buckler, E.S., and Martienssen, R. (2005). Architecture of floral branch systems in maize and related grasses. Nature **436:** 1119–1126.

Yamaji, N., and Ma, J.F. (2014). The node, a hub for mineral nutrient distribution in graminaceous plants. Trends Plant Sci. **19:** 556–563.